Thermal finite element modelling of the SMOG-1 nanosatellite

Balázs Petróczi

Supervisor:

Viktor Józsa

Budapest, 2016

1   Acknowledgement

First of all, I would like to thank dr. Gschwindt András for the opportunity to attend the project, without his tireless work there would not be the SMOG-1.

Special thanks to Viktor Józsa for helping through the difficulties. In particular, to correcting my mistakes which could have caused sleepless nights.

I also wish to thank Levente Dudás help for the explanation of the electrical components and that he followed through my work.

I received a lot of help from: Emil Viktor Hödl for the orbital calculations and the battery parameters, Tibor Herman for the CAD geometry and last but not least Timur Kristóf for his advice on my paper.

Contents

2 Introduction and content

The SMOG-1 is a pocketqube class -50x50x50mm cube- nanosatellite, developed at the Budapest University of Technology and Economics by electrical and mechanical engineering students. My task within the SMOG-1 research and development team was the satellite thermal modelling by finite element method. The aim of my paper besides participating in the 2016 Scientific Students' Associations is that I wanted to document my work in order to provide evidence that I completed the task entrusted to me with proper caution. In addition, others can learn from my work regardless of the mission eventual success or failure. The content of this document -after the introduction of the SMOG-1 mission, geometry, and structure- can be divided into three main parts. A brief summary of the main parts are listed below:

1. Chapter 3 is mainly based on a literature survey. In this chapter, we discussed basic thermodynamic concepts which at first may seem trivial to the reader but it is necessary in order to introduce the fundamental concepts of space thermal engineering. By the end of the chapter, the reader will be familiar with the basic concept and thermal effects occurring in space and fully understand the importance of the next two chapters where we define the thermal environment of the satellite.

2. The fourth and fifth chapter is about the SMOG-1 orbit and its thermal environment. The orbit path is calculated by the STK AGI software package and we need this only to calculate the thermal environment, therefore, the orbit overview is non-exhaustive. At this point, the reader will have a clear image of the satellites position and thermal load around Earth.

3. From the sixth to the last section we build up the satellite's model step by step in Ansys software environment and use the gained information to thermally insulate the problematic component(s). The reader is guided through the process of thermal modelling.

Generally, the available literature data of satellite thermal design is vast. However, it is thin in the case of the new generation small-sized satellites. Therefore, the present work may contribute to the success of other missions and adds a considerble value to the thermal design of PocketQube-class satellites.

3 SMOG-1

3.1 Mission and goals

The primary mission of the satellite is the monitoring of the electromagnetic radiation in low Earth orbit in the DVB-T terrestial digital TV broadcasting bandwidth (430-860 MHz).[1] Now, why would anyone want to do that? The antennas of commercial broadcasting companies today are far from ideal, so they radiate towards not only the customers but also to space. The unused power can be considered as a loss called: electrosmog. With the monitoring of this lost power, we can identify it's magnitude and distribution below the satellite. The resulting data then can be used to improve the efficiency of DVB-T antennas.

In addition, the satellite has radiation dosimeters which measures the total radiation dose of ionizing high-energy particles. This components monitors the satellite gamma radiation exposure which is important because this radiation can cause damage to electronic components which may reduce the lifetime of the satellites.[2] [3] [4] [5]

Because the functional lifetime of the satellite is estimated to be less than the time the satellite return to the atmosphere and burn, magnetic plates have been fixed to the outer surface of the satellite to slow down the structure. The lifetime of the satellite in our orbit is estimated to be 10 years while the mission can be completed within one year. Knowing that other two satellites also leave with us and they are in the same orbit as us with minimal deviation, we can observe if this magnetic sheet really slows us down compared to them. Also, the screws holding together the satellites PCB's are made of magnetic material in order to decrease the angular velocity of the structure.

3.2 PocketQube

The first standard proposed by Bob Twiggs was the 1U CubeSat with a nominal side length of 10 cm with maximum mass of 1 kg. The first Hungarian satellite, the MaSat-1 was of such size. Next, the aim was to reduce and standardize the size of the satellites in order to lower launch costs thus making it affordable for students in universities and independent groups. With the increased demand and price, emerged the need of an even smaller satellite to significantly cut launch costs. Thus, the 1p size PQ framework was designed cutting the launch cost to 20000$. A 1p PocketQube is a cube with 5 cm nominal side length, and maximum weight of 250 g. Additional components can be placed into a 7 mm shell around the cube, showed by an opaque tan shell around the satellite, in figure

1.[6][1] The orange plate is the back plate of the satellite. Via this plate, the satellite is
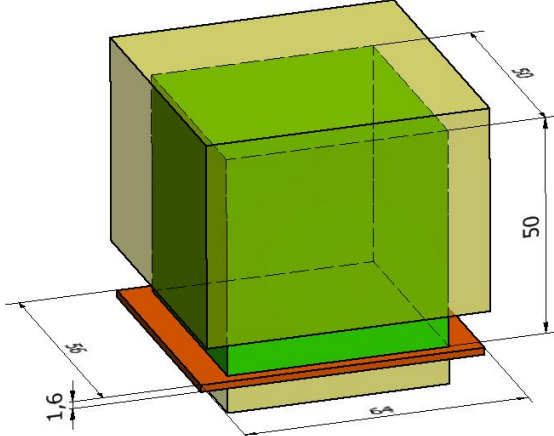

Figure 1: PocketQube overall dimensions

connected to a rail which is located inside the deployer. This has a spring which is in a pre-stressed state when all the satellites are loaded and the ejection door is closed. After the payload is in space, and the ejection door is opened the satellites are then pushed out by the spring. These deployers are usually fitted as a secondary payload beside a usually large commercial or scientifican satellite. In our case, we and other two satellites will launched onboard the UniSat-7 which is developed by GAUSS Team. The estimated launch of the UniSat-7 is the beginning of the second half of 2017 launched by a Dnepr launch platform. So, in summary: three small satellites including the SMOG-1 are loaded into the MRFOD (pocketqube deployer). This deployer is onboard in the UniSat-7 which is launched by the Dnepr launch platform.

Already a lot of cube CubeSats is in space and from some of their documentation of thermal analyses are available which provided a good basis to carry out the thermal design of SOMG-1.[7][8][9][10] Also, there are available some articles about the CubeSats.[11][12] Nevertheless, similar analysis is not available for the public according to the best knowledge of the author. Consequently, the cited documents provided a good basis to start, especially the *Thermal Design of the Oufti-1 nanosatellite* by Lionel Jacques, which discuss the matter in a great detail.[14] Furthermore, before this paper, two other students also worked on the thermal modeling of the SMOG-1 by examining different arrangements and they wrote a paper about it in 2014. But, since then a lot has changed in the structure of the satellite.[13] Overall, all of the cited work was a very great help to get started and they deserve great thanks for their documented work.

---

[1]It should be noted that the actual size constraints of SMOG-1 are slightly differs from the illustrated image, but since the contract is confidential it can not be presented here.

3.3   Structure of the satellite

The structure is entirely made of circuit boards. The side panels with the internal PCB's join together like a puzzle box, top and bottom panels connect to this via tabs. These panels are jointed by two M3 threaded rods holding the panels togeather. The exploded view of SMOG-1 is shown in figure 3., where the panels are:

- Primary EPS: primary electrical power system developed by Tibor Herman. This subsystem is responsible for collecting the energy generated using 6 solar cells placed on the six sides of the cube. The solar cells are mounted on a PCB panel and on the opposite side of the PCB panel is a maximum power point tracking circuit (MPPT) which maximizes the absorbed power of the solar cells. This is connected to the central EPS through the unregulated power bus. [3]

- Central EPS: central electrical power system developed by Gábor Géczy, is responsible for energy regulation and distribution it converts the raw power coming from the solar cells into a stable 3.3V (regulated power bus). Furthermore, this system manages the battery which is located at the free side of the COM board.[5] It consists of two PCB panels. Panel A is responsible for power regulation, and Panel B contains the battery management circuit and the total ionizing dose sensor (TID).

- COM: satellite communication with the ground station, developed by Levente Dudás. It is responsible for satellite communication with the ground station and radio amateurs all over the world and also for accomplishing our primary mission, the spectrum analysis.

- OBC: onboard computer developed by Timur Kristóf. It controls all the satellite subsystems, collects information from the measurement instruments and telemetry from every other subsystem.

- Antenna deployer: in undeployed state, the antennas are tied to the satellite with a plastic line also tied to resistors. When the antenna is about to be opened, the resistors heat up and melt the plastic.[2]

The engineering sample of the SMOG-1 is shown in 2, showing its framework. Currently, only one solar panel is fitted to the satellite. My task in the team is the thermal subsystem design. It means that there is a operability limitations for all components in which the real case must fit in. These values for the main components are shown in table 1. Due to limitations in size and the components to include are given, the designer has low degree of freedom to tailor each component together with by providing an appropriate thermal
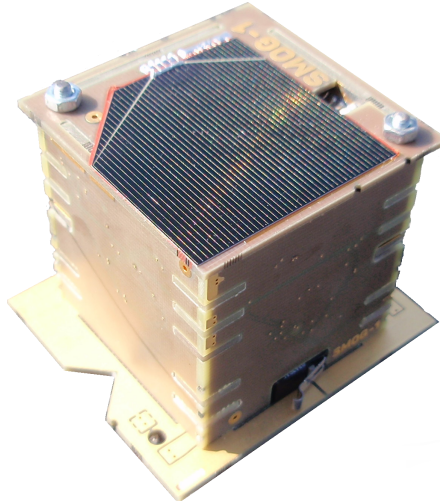
Figure 2: The SMOG-1 engineering copy with one solar cell.

Component	Maximum temperature $°C$	Minimum temperature $°C$
Electronics	80	-40
Battery, charging	45	0
Battery, discharging	60	-10
PCB	130	$-$

Table 1: Operation temperature limits

environment for each of them. As a consequence, the present paper mainly focuses on the most sensitive component, the battery.
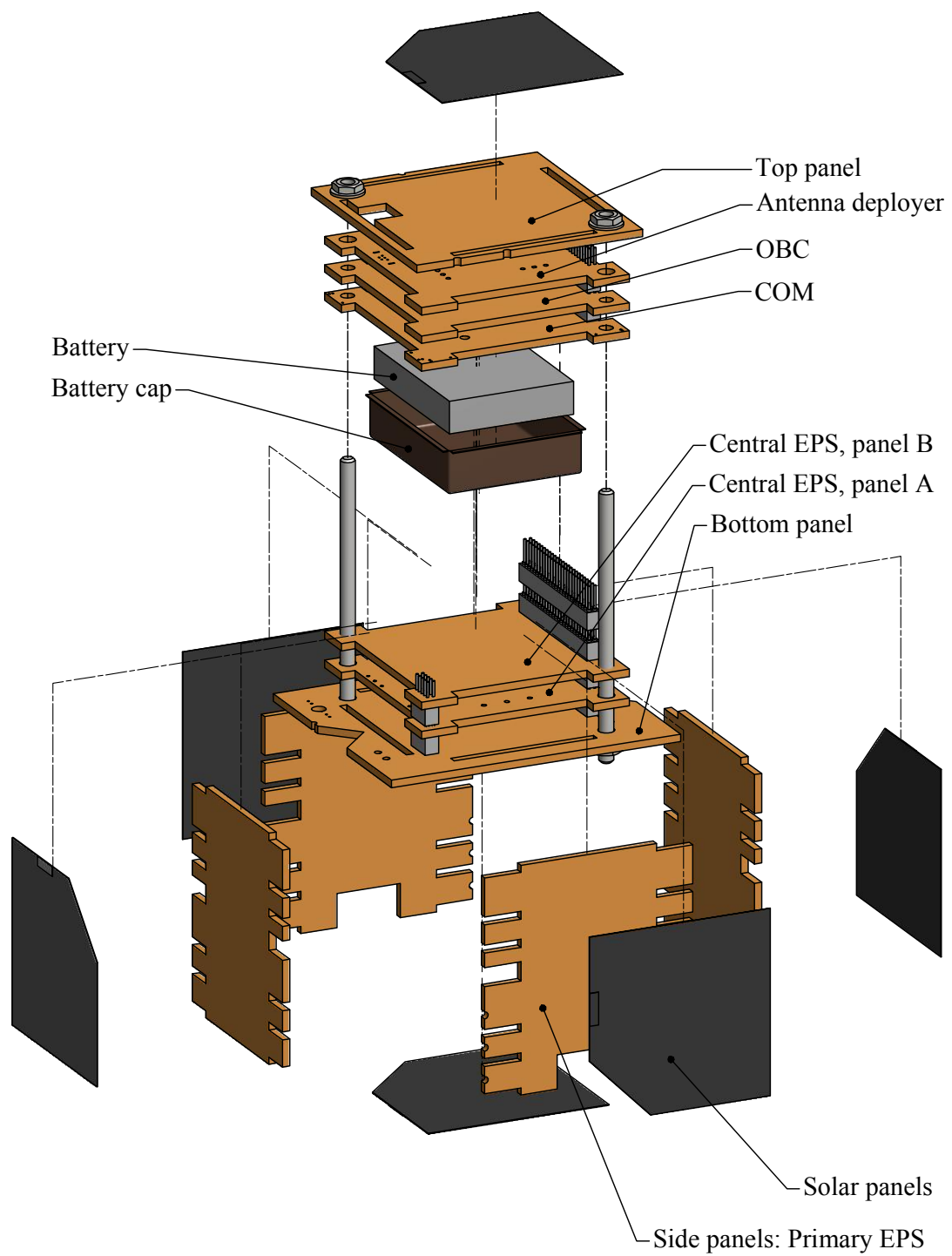
Figure 3: Exploded view of SMOG-1

4 Space environment

Space is a hazardous environment both for man and machine due to: radiation, plasma, micrometerioites, space debris, vacuum and so on. Most of the environmental effects are unpredictable which makes even harder to prepare for them. From a thermal engineers point of view, the main problem is the extreme temperatures of the satellite systems. While a satellite is in the shadow of the Earth can easily go below sub-zero centigrade temperatures and when the sun is visible, it can go up to very high temperatures which can cause component or even mission failure. So the task is to ensure that no components exceed their critical minimum and maximum temperatures. In order to calculate and design the appropriate thermal subsystems, we have to understand these effects. In this chapter, we review the basic thermal effects present in space.

4.1 Heat transfer in space

We distinguish three kinds of heat transfer modes on Earth: convection, conduction, and radiation. However, in the vacuum of space, there is no heat convection, only the latter two heat transfern mode play a role.

4.1.1 Conduction

When the heat in a continuous solid material propagates from the warmer side to the colder. This phenomenon heavily depends on the material properties. In the case of metallic materials, the heat energy travels by the vibrations of the atoms in the crystal lattice and with the diffusion of free electrons. In non-metallic materials and fluids, happens through flexible elementary waves. Fourier's law describe the mathematical form where the heat flow rate is equal to the condoctivity times the gradient of the temperature field as follows[15]:

$$\underline{\dot{q}} = -\lambda \nabla T \tag{1}$$

4.1.2 Thermal radiation

All material with temperature greater than zero kelvin radiate electromagnetic waves. These waves can be absorbed by other bodies and increase their temperature that leads to an amplified electromagnetic wave emission. The electromagnetic waves can be absorbed, reflected, and transmitted. The sum of these factors is always equals to one:

$$\alpha + \rho + \tau = 1 \tag{2}$$

where:

- α is the absortivity,

- ρ is the reflectivity,

- τ is the transmissivity.

The radiation intensity of a black body (α=1), per unit solid angle for a specific wavelength is defined by Planck's law:

$$I^e_{\lambda\omega,0} = \frac{1}{\lambda^5}\frac{2hc^2}{e(hc/\lambda Tk) - 1} \tag{3}$$

where:

- $c = 2.998 \ 10^8 \ m/s$ is the speed of light,

- $h = 6.625 \ 10^{-34} \ Js$ is the Planck's constant,

- $k = 1.38 \ 10^{-23} \ J/K$ is the Boltzmann constant.

By integrating equation (3) on the entire wavelength range yields the black body emitted energy per unit surface area known as the Stepfan-Boltzmann law:

$$E^e_0 = \int\limits_0^\infty \pi I^e_{\lambda\omega,0}d\lambda = \sigma_0 T^4, \tag{4}$$

where:

- $\sigma_0 = 5.67 10^{-8} W/(m^2 K^4)$ is the Stefan-Boltzmann constant,

- T is the temperature of the black body,

- λ is the wavelength.

This is affected by the emissivity and the view factor. The emissivity is the ratio between the radiation of a material and its corresponding black body radiation, which can be dependent on wavelength and the incidence of the radiation. If the emissivity is wavelength and direction independent, we call it grey body and the Stepfan-Boltzmann law can be used to derive the emitted energy per unit surface area:

$$E^e = \varepsilon\sigma_0 T^4 \tag{5}$$

where $\varepsilon < 1$. Thus, we can assume that the body emissivity is constant at all wavelengths. However, this is not true, the emissivity of materials can be greatly wavelength dependent. In order to take this into account, generally the space industry uses two constant emissivities:

- α Short-wave absorbance. The constant emissivity below $3\mu m$ wavelengths.

8

- ε Long-wave emittance. The constant emissivity above $3\mu m$ wavelengths.

This can be done due to the fact that the spectral distribution of the radiation from the Sun and the reflected sunlight from the Earth's atmosphere is below $3\mu m$, while the Earth infrared radiation is above $3\mu m$.[16] This spectral distribution is on figure 4. Kirchoff's law states that in any specific wavelength and direction, the emissivity is equal to the absorptivity, thus: $\varepsilon(\lambda) = \alpha(\lambda)$. Of course, this also applies to our case too, therefore, to avoid confusion, the short-wave absorptance is equal to the short-wave emittance and the long-wave emittance is equal to the long-wave absorbance. In the upcomings, we refer to them as they were shown above.
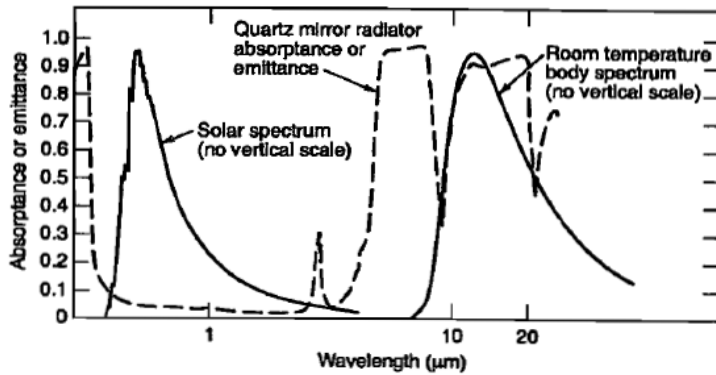

Figure 4: Wavelength dependence of various bodies.[19]

4.1.3   View factor

Another important part of the thermal radiation between two surfaces is the view or the shape factor. Between two surfaces, noted by F_1 and F_2 the radiative heat follows the Lamberts law, stating that the directional emissivity is proportional to $\cos(\phi)$ where ϕ is the angle between the surface normal and the direction of the radiation. The view factor between F_1 and F_2 can be calculated as follows::

$$\phi_{12} = \frac{1}{\pi F_1} \int\limits_{F_1} \int\limits_{F_2} \cos\phi_1 \cos\phi_2 \frac{dF_1 dF_2}{r^2} \tag{6}$$

This equation (6) only depends on geometries and their orientations. This calculation can very difficult but in the literature, there are diagrams which we can use to get the view factor of the satellites surface viewed from Earth, one of this diagram is on figure 5. Later in section 7, the modelling, we will use this to determine the view factor for different arrangements. As for a short summary:

- In space, the considerable heat propagation modes are heat conduction and thermal radiation.
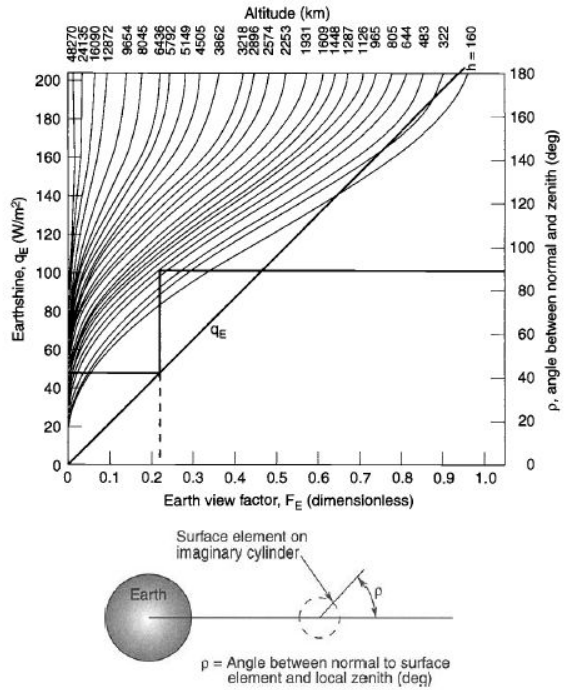
9

Figure 5: View factor from Gilmor's Thermal Control Handbook.[18]

- We assume that all the surfaces of the satellite follow the Lambert's law.

- Deviation from the usual, we use two emissivity factors: shortwave(SW) absorbance(α) and longwave(LW) emittance(ε) through in this paper.

- For the view factor, we will use the 5 diagram from Gilmore's Thermal Control Handbook.[18]

4.2   Introduction of the thermal environment

The the heat source of the satellite in low earth orbit are the direct solar sunlight, the reflected solar sunlight by the Earth surface as well as by the atmosphere. This effect is called as albedo radiation and Earth infrared radiation, showed in figure 6. These
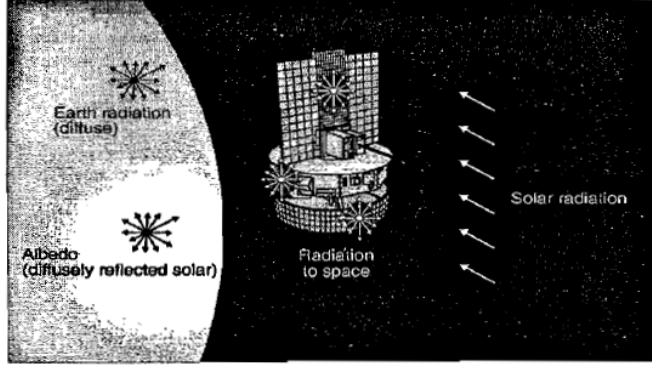

Figure 6: Thermal environment[19]

factors are added up to the internally generated heat by the operation of the electronic components. While the heat loss occurs due to the radiation to the cosmic background which can be modelled as a 2.7 K temperature black body.[19] [20]

4.2.1   Solar radiation

The radiation coming from the Sun is the main heat source of a satellite. The level of the incoming radiation from the sun is affected by the distance from the sun and can be calculated from its characteristic black body temperature. Of course, the power given off by the solar radiation is not constant, from measurements, we know that there are random and seasonal fluctuations.[21] [22] Distance of the Earth-orbiting staellite from the Sun can assumed as the Sun - Earth distance. This also changes as the Earth elliptical orbit aphelion is 152.1 $10^6 km$ while it's perihelion is 147.1 $10^6 km$. The mean value of the sun irradiance is $S_0 = 1367 W/m^2$. Taking into account the above-mentioned effects a minimum and maximum value was measured as[16]:

$$S_{min} = 1322 \frac{W}{m^2}$$
$$S_{max} = 1415 \frac{W}{m^2}$$

(7)

4.2.2   Albedo radiation

The albedo is a fraction of the sun radiation reflected or scattered by the Earth's surface and atmosphere. This also occurs as an SW incoming heat flux to the satellite. In order to avoid confusion, we call the former as albedo factor and the latter one as albedo radiation

11

and do not use the word itself: albedo. The albedo factor:

$$a = \frac{q_r}{S\cos(\Theta)} \tag{8}$$

where:

- a is the albedo factor,

- q_r is the magnitude of the reflected SW radiation at the top of the atmosphere in W/m^2,

- S is the direct solar radiation W/m^2,

- Θ is the solar zenith angle: the angle between the earth-sun vector and the zenith angle shown in figure 8.

In general, the albedo flux tends to be lower as we move to the north and south poles and reach the highest value when the sun exactly above us i.e. $\Theta = 0$, because the heat flux per unit area is lower going towards the poles. While the albedo factor increases on higher latitude. The main reason behind this is that on higher latitudes the sun rays pass through a longer section of the atmosphere thus increasing the scattered radiation. However, this can only be said in general, because the albedo factor significantly affected by the surface type, cloud formations and by the weather. Above the poles and deserts, the albedo factor is higher while above continental and oceanic areas it tends to be lower.[19] [16]

4.2.3 Infrared radiation of the Earth

The Earth emits infrared LW radiation and can be characterized as a 288 K temperature black body. This is the only heat source which is always present even when the satellite is in the Earth's shadow. It does not change as strongly as the albedo, but it is lower in higher latitudes due to the lower temperatures through the poles while higher near the equator and desert areas where the surface temperature is higher.

4.2.4 Aerotermal flux

The aerothermal flux is the heat from collision and friction with remnant molecules in the atmosphere. It is negligible in the orbit of the SMOG-1.[19]

5   The orbit of SMOG-1

In this chapter, we present the SMOG-1 orbital path around Earth. The calculation of the orbit is an indirect task since it determined the incoming heat fluxes, therefore, significantly affects the thermal equilibrium of the satellite. What we need is the altitude, solar zenith angle and the orbital time of the satellite. The STK AGI software package was used to determine these parameters. The SMOG-1 will be in a low earth orbit(LEO). Figure 7. shows the range of the LEO which ranges from 160 km altitude to 2000 km. The solar zenith angle is the angle between the sun-earth vector and the earth-satellite
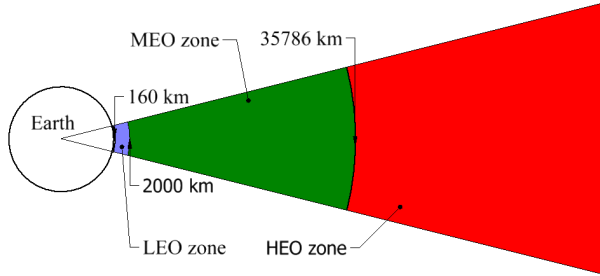

Figure 7: The low, medium and high earth orbit. The blue stripe symbolizes the low earth orbit, the green medium earth orbit and the red is the high earth orbit, the values are altitudes.

vector showed in figure 8. The importance of this that it directly influences the albedo radiation. The SMOG-1 will be on an elliptical so-called sun synchronous orbit (SSO).
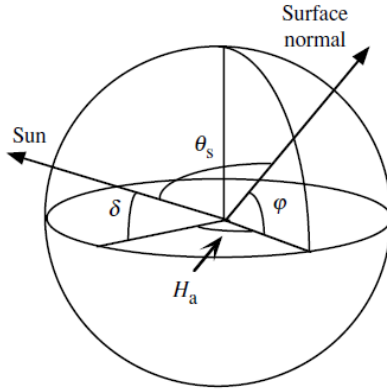

Figure 8: The representation of the solar zenith angle: Θ_s. The surface normal is the direction of the zenith and point to the satellite.[24]

The peculiarity of such an orbit is that the satellite local solar time on its path projected to the surface is always the same. In other words, the satellite always passes over the equator at a given time.This happens because the extra weight around the equator causes the precession of the orbital plane. This can be achieved by the appropriate configuration

of the orbital inclination and altitude. This is high, more than 90° inclination retrograde orbits. The classical orbital elements are the necessary parameters which describe the satellite orbit shown on figure 9 and 10, the simbols [23]:

- t_0 epoch time: is the Julian day and GMT time, in fact, the initial time.

- a semi-major axis: is the half of the ellipse main axis, shown on figure 9.

- e eccentricity: is the degree fo ellipticity.

- i inclination: is the angle between the equatorial and orbital plane 10.

- M_0 mean anomaly: is the angle from one of the focus to the mean circle of the elliptic.

- Ω_0 Right ascension of ascending node: is the angle between the vernal equinox and the ascending node measured eastward.

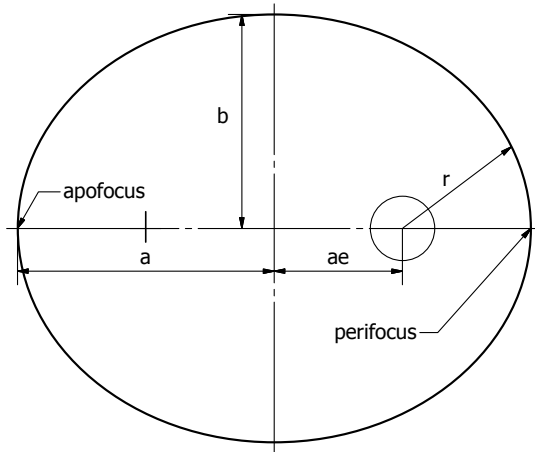- ω_0 argument of perigee: angle in an orbital plane from the ascending node to the perifocus.

Figure 9: Parameters of the elliptical orbit elements

While we did not get all of the classical orbital elements in the contract with GAUSS, it is suffice to determine the orbit by approximating the missing elements (the approximation does not effect significantly the orbit)[2]. The simulation start time is the second half of 2017, currently this is the launch time of the satellite. The satellite orbit is on figure 11. This is a scale figure so you may want to take a good look at it, as it shows how close the satellite to the surface. We can draw some conclusions from this such as the

---

[2]It should be noted that the actual orbital elements can not be provided because the contract is confidential.
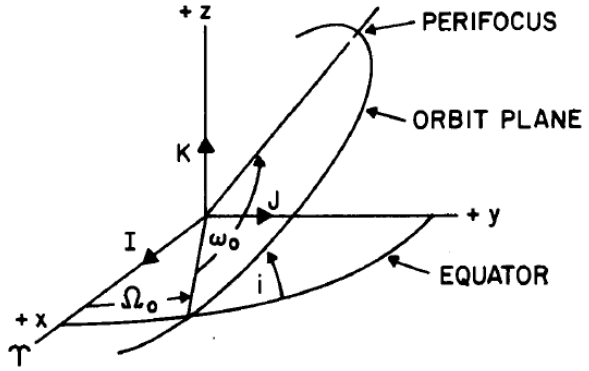
Figure 10: The classical orientation angles and the orthogonal I, J, K coordinate system.[23]

satellites see the Earth in a high angle, thus the effect of the SW albedo and Earth LW radiation is strong. While it blurred out the albedo radiation surface dependency. From
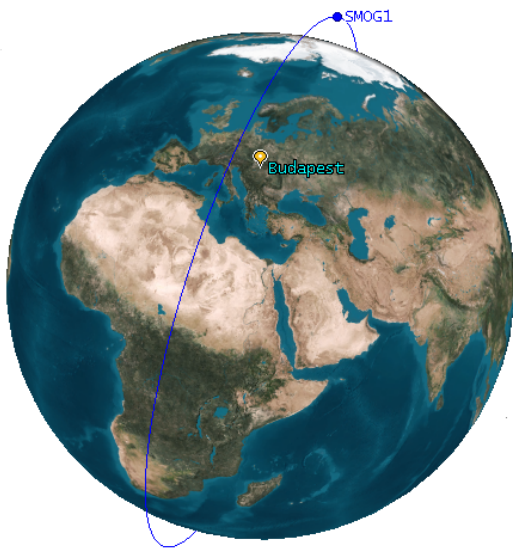
Figure 11: SMOG-1 scale orbit, picture from STK AGI software.

the simulation, we can save out the orbital period and shadow time as well as the altitude and the solar zenith angle. The total time of one orbit is 96 minute. From the total time 38 minute, roughly 40% is in the Earths shadow. Later this will very important for the simulation in order to switch off and on the sun and albedo radiations. The altitude and the solar zenith angle variation by time is on figure 12. and 13.

Figure 12: Altitude by time

Figure 13: Solar zenith angle by time

6 Thermal environment of an orbit

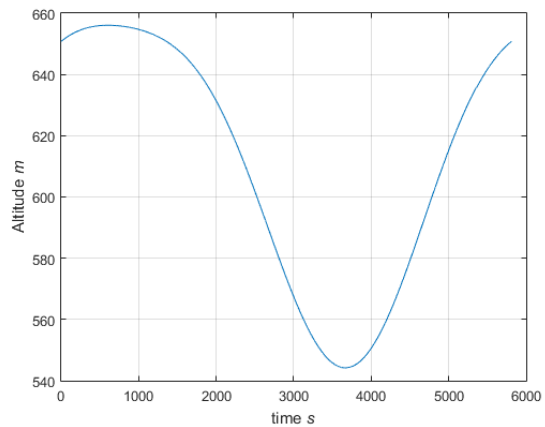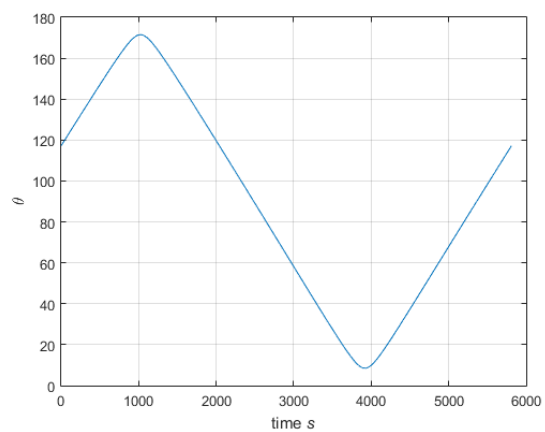Now everything is given to determine the thermal environment of the satellite orbit. Often the thermal fluxes that reach the satellite are calculated from simple averages. The Earth can be modeled as a 288 K temperature black body, the mean solar flux is 1367 W/m^2 and the mean albedo factor is 0.3. However, since the satellite is in a high inclination orbit, thus passes above sites where the albedo factor is high while the earth radiation is low and other places where the opposite it would not necessarily be a good approximation using the average values. Especially since the small size of the satellite makes it highly sensitive to rapidly changing thermal radiation fluctuations. Of course it is, very difficult to choose appropriate parameters. Suffice it to say that the earth radiation varies from area to area not to mention the albedo factor which is affected by unpredictable events. However, through the Earth Radiation Budget Experiment(ERBE) there are available measurement data from the outgoing SW and LW fluxes of Earth. These measurements are summarized in the „Simple Thermal Environment Model"(STEM) published by NASA. [17] From, the minimum and maximum values can be selected for a given orbit. Hence we can count on real measured values which incorporate the random climatic effects and the dependence on the local disturbances. The calculations of the near-Earth thermal parameter selection are based on these instructions. The primary goal of the ERBE is to monitor the earth radiation and determine the monthly average radiation of Earth. The mission is still ongoing by three satellites:

- NOAA-9, altitude: 849 km,$i = 99°$,

- NOAA-10, altitude: 815 km,$i = 99°$,

- ERBS, altitude: 610 km,$i = 56°$.

All the satellites are equipped with narrow and wide field-of-view active cavity radiometers. The wide field of view measurements was used for STEM because it measures more directly the SW and LW irradiances that effect the satellite surfaces. We have shown in the previous chapters what the albedo and earth infrared radiation depend on but it is also worth checking out a few things shown in STEM. Figure 14. shows the ERBS satellite measured albedo factor and outgoing LW radiation(OLR) pairs. It can be seen how large the difference is over different areas. Without going into a deeper detail, on the measurement data, they set up hot and cold cases of albedo factor and OLR pairs, based on averaging times and orbital inclination seen in table 2. These are all corrected values to the top of the atmosphere. The top of the atmosphere(TOA) is a theoretical surface above the earth radius by 30 km. This is the area where we assume that the outgoing radiation is homogeneous and perpendicular to the surface. Furthermore, at this level, the thermal
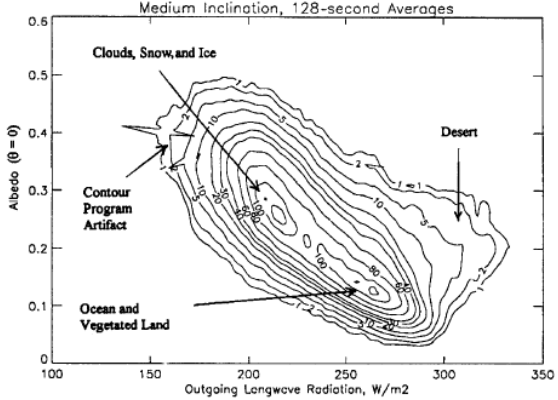
Figure 14: Contour of ERBS-observed frequency of TOA albedo(at solar zenith angle 0) and outgoing LW radiation(OLR): 128 second averaging time, medium inclination orbit.[17]

radiation emitted by the earth may no longer significantly influenced by the atmosphere. The averaging time is the time period of the averaged data. The albedo hot and cold extreme environment at a given orbital inclination is the maximum or minimum albedo factor paired to the averaged OLR while the OLR hot and cold extreme environment at a given orbital inclination is the maximum or minimum OLR value paired to the averaged albedo factor. The combined hot case defined as the albedo factor and OLR pair where 0.04 percent of the measured data is higher while the cold case is where 0.04 percent of the measured data is lower than that. In order to select the appropriate values for our orbit from table 2, we have to choose an averaging time and an extreme type. We know that our orbital inclination is $i = 98°$, thus it is in the range of the inclination, namely between $60 - 110°$. The extreme type depends on the satellite surface absorptivity and emissivity. The satellite is covered with solar cells, one solar cell area is $1509mm^2$. Roughly 60% of the satellite surface is covered by solar cells, the other 40% the plain FR-4 without the green solder lacquer. The solar cell emissivity and absorptivity are given in the data table, however, for the clean PCB we do not know that. Since there is no chance to measure it we use the fiberglass emissivity, in both the SW and LW range, the values are in table 3. For example, if the absorptivity is higher then the emissivity thus takes up more heat from SW radiation than the LW radiation the extreme type is albedo. Because it will take up the most heat from albedo radiation therefore in hot case the albedo factor is the highest while in cold case the albedo factor is the lowest. In general, the evaluation method is to calculate the incoming heat fluxes for all of the albedo/OLR pairs, comparing them and selecting the worst case. Before we do this, one must understand that the data shown in table 2. is for TOA and the solar zenith angle zero. This means that we will have to calculate both Earth infrared radiation flux and the albedo flux at our altitude by using

Ext. type	Avg. time	Mission critical cold case						Mission critical hot case					
		0 − 30°		30 − 60°		60 − 110°		0 − 30°		30 − 60°		60 − 110°	
		Alb	OLR	Alb	OLR	Alb	OLR	Alb	OLR	Alb	OLR	Alb	OLR
Alb	16 s	0.06	273	0.06	273	0.06	273	0.43	182	0.48	180	0.50	180
Alb	128 s	0.06	273	0.06	273	0.06	273	0.42	181	0.47	180	0.49	184
Alb	896 s	0.07	265	0.08	262	0.09	264	0.37	219	0.36	192	0.35	202
Alb	30 m	0.08	261	0.12	246	0.13	246	0.33	219	0.34	205	0.33	204
Alb	90 m	0.11	258	0.16	239	0.16	231	0.28	237	0.31	204	0.28	214
Alb	6 h	0.14	245	0.18	238	0.18	231	0.23	248	0.31	212	0.27	218
Alb	24 h	0.16	240	0.19	233	0.18	231	0.22	251	0.28	224	0.24	224
Comb	16 s	0.13	225	0.15	213	0.16	212	0.30	298	0.31	267	0.32	263
Comb	128 s	0.13	226	0.15	213	0.16	212	0.29	295	0.30	265	0.31	262
Comb	896 s	0.14	227	0.17	217	0.17	218	0.28	291	0.28	258	0.28	259
Comb	30 m	0.14	228	0.18	217	0.18	218	0.26	284	0.28	261	0.27	260
Comb	90 m	0.14	228	0.19	218	0.19	218	0.24	275	0.26	257	0.26	244
Comb	6 h	0.16	232	0.19	221	0.20	224	0.21	264	0.24	248	0.24	233
Comb	24 h	0.16	235	0.20	223	0.20	224	0.20	260	0.24	247	0.23	232
OLR	16 s	0.40	150	0.40	151	0.40	108	0.22	331	0.21	332	0.22	332
OLR	128 s	0.38	154	0.38	155	0.38	111	0.22	326	0.22	331	0.22	331
OLR	896 s	0.33	173	0.34	163	0.33	148	0.22	318	0.22	297	0.20	294
OLR	30 m	0.30	188	0.27	176	0.31	175	0.17	297	0.21	282	0.20	284
OLR	90 m	0.25	206	0.30	200	0.26	193	0.20	285	0.22	274	0.22	250
OLR	6 h	0.19	224	0.31	207	0.27	202	0.19	269	0.21	249	0.22	221
OLR	24 h	0.18	230	0.25	210	0.24	205	0.19	262	0.218	245	0.20	217

Table 2: Albedo (at solar zenith angle zero) and OLR values for mission-critical hot and cold case extreme environments at low, medium and high inclinations, and averaging intervals from 16 seconds to 24 hours. Albedo type extremes are labeled „Alb".[17]

Surface	α	ε	References
fiberglass	-	0.7	[33]
Solar cell	0.83	0.95	[34]

Table 3: Material data

equation (9). This equation is simply derived from the proportion of the spheres which radius is equal to the earth radius plus the TOA(30 km) height and the sphere with the radius of the earth plus the altitude of the satellite.

$$q_a(r_a(t)) = q_T OA \frac{r_{30}}{r_e + r_a(t)} \tag{9}$$

where:

- q_a heat flux in a given altitude

- $q_T OA$ heat flux in the TOA altitude

- r_{30} the altitude of the TOA which is 30 km

- r_e Earth radius which is 30 km

- $r_a(t)$ satellite altitude 6371 km

The albedo factor is independent from solar zenith angle, thus we have to correct it by the „c" cerrection factor using 10.

$$a(\Theta(t)) = a_0 + c(\Theta(t)) \tag{10}$$

The a_0 is the albedo factor chosen from table 2. The „c" is the cerrection factor which depends, on the solar zenith angle. Of course, the solar zenith angle depends of the satelite positon hence varies with time. The correction factor can be calculated from equation (11).

$$c(\Theta(t)) = c_1\Theta(t) + c_2\Theta(t) + c_3\Theta(t) + c_4\Theta(t) \tag{11}$$

where:

- $c_1 = 1.3798 \cdot 10^{-3}$

- $c_2 = -2.1793 \cdot 10^{-5}$

- $c_3 = 6.0372 \cdot 10^{-8}$

- $c_4 = 4.9115 \cdot 10^{-9}$

For the comparison, we do not have to calculate to our orbital altitude with equation 9, it will be required later. However, the albedo flux in order to be comparable we have to calculate an average value from the time-dependent flux. This can be carried out by averaging of the $a(\Theta(t))$ over one orbital period, P. The average albedo factor:

$$\overline{a} = a_0 + \overline{c} \tag{12}$$

Where $\overline{a}$ is the averaged albedo factor and $\overline{c}$ is the averaged albedo correction factor, which calculated from equation (13).

$$\overline{c} = \frac{\int\limits_0^P c(\Theta(t))\cos(\Theta(t)dt}{\int\limits_0^P \cos(\Theta(t)dt} \tag{13}$$

Substituting our orbital zenith angle showed in figure 13 into equation 13 then to equation (11) yield the averaged albedo any value in table 2. Using up the surface ratio between the plain FR-4 and the scale cell on one side of the cube, we can evaluate the data in the table by equation 14 and 15.

$$q_{SW} = 0.6\alpha_{sc}S\overline{a} + 0.4\alpha_{PCB}S\overline{a} \tag{14}$$

$$q_{LW} = 0.6\varepsilon_{sc}q_e + 0.4\varepsilon_{PCB}q_e \tag{15}$$

where:

- α_{sc} and α_{PCB} is the absorptivity of the solar cell and the PCB,

- ε_{sc} and ε_{PCB} is the emissivity of the solar cell and the PCB,

- the 0.4 and 0.6 multipliers are the ratio between the solar cell and the PCB plain surface,

- q_e and $\overline{a}$ are the OLR and corrected average albedo factor pairs.

By evaluating this, of course, it is not a surprise that the maximum and minimum values are in the combined extreme type because the PCB absorptivity and emissivity ratio is $\alpha_{PCB}/\varepsilon_{PCB} = 1$, while the solar cell ratio is $\alpha_{sc}/\varepsilon_{sc} = 0.87$. Consequently, the surface of the satellite gets about the same amount of energy from SW and LW fluxes. With regard to the averaging time, STEM suggests that a base line should be chosen from long avereges and small averages should be added to this base value as pulses. However, we deviate from that and only use the 16 secound data without pulses in order to examine the worst case scenario. So, in summary, we have to chose from the high inclination, combined case where the average time is 16s. The selected values for the hot and cold case is highlighted in table 4. Now, using this, we can calculate the albedo and earth

-	Albedo factor	Earth radiation flux	Solar radiation flux
Cold case	0.16	212	1317
Hot case	0.32	263	1419

Table 4: The chosen near earth values

infrared radiation flux. With the maximum and minimum solar irradiance (7), corrected albedo (11), and altitude correction (9), we can calculate the SW fluxes by equation: (16) and (17).

$$q_{SW_{min}} = S_{min} a(\Theta(t)) \frac{r_{30}}{r_e + r_a(t)} \tag{16}$$

$$q_{SW_{max}} = S_{max} a(\Theta(t)) \frac{r_{30}}{r_e + r_a(t)} \tag{17}$$

The LW fluxes: (18) and (19).

$$q_{LW_{min}} = q_{e_{min}} \frac{r_{30}}{r_e + r_a(t)} \tag{18}$$

$$q_{LW_{max}} = q_{e_{max}} \frac{r_{30}}{r_e + r_a(t)} \tag{19}$$
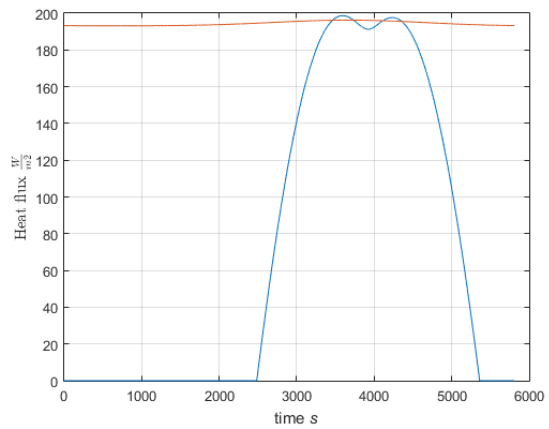
Figure 15: Cold case albedo(blue) flux and Earth infrared(red) radiation for one orbitalperiod.
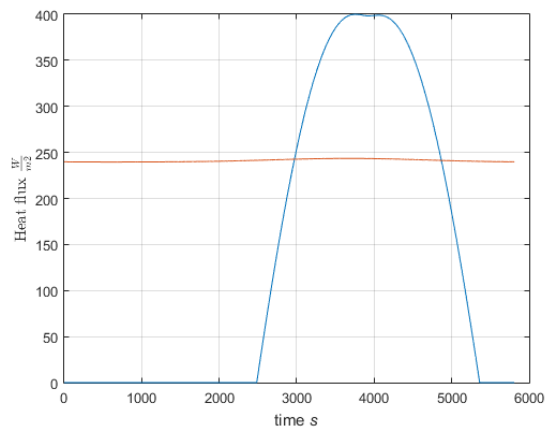

Figure 16: Hot case albedo(blue) flux and Earth infrared(red) radiation for one orbitalperiod.

7 FEM analisys

We used the Ansys software environment for all of the simulations provided by the department. At first, simpler models were examined. These simulations were based on older satellite modells which is now obsolete and we used simpler boundary conditions, but these are also out of date compared to the Earth modell discussed in Section 6. So they do not help in the design of the insulation, for this reason, they are not included in the thesis. But I would mention that, overall, the experience gained during this time contributed to the whole project because I learned what mesh size and time step should be used in transient thermal analysis of the satellite. Thus before the more important simulations, I already know what mesh and time stepping should be used in order to avoid the too much solving time and the result becomes mesh and time independent. The FEM analysis is divided into two sections: the first one is the insulation and battery placement considerations by utilizing the above calculated thermal environment on the simple modell of the satellite. We look at a variety of layouts with different insulation and examine how it affects the temperature of the battery. Secondly, on the detailed modell of the satellite with refined material characteristics, examine the assembled insulation by a larger averaging time albedo-OLR pair in order to estimate the temperature distribution in space with a higher accuracy.

7.1 Preliminary FEM analisys

In the following, we present the model in which we performed the calculations. First, the geometry, meshing, and the boundary conditions are presented which are not changed during the various simulations in this chapter. Those parameters that are altered will be discussed in the subchapters.

7.1.1 Geometry

The model geometry is derived from the CAD modell of the satellite made by Tibor Herman, shown in figure 17a. The model includes dimensions of the satellite with several electronic components soldered to their host panels, including the solar cells. However, these components are practically unnecessary for the simulation, therefore, they were removed from the model. It is not trivial that the solar cells should be neglected or not. As a consequence, the following calculation helps us to find out its importance. Firstly, determining the heat capacity of one side then compare it to the distinct parts: The solar cell is a triple junction GaAs solar cell which neither the conduction nor the specific heat is known, for this reason, we used the gallium arsenide(GaAs) material properties. The thermal conductivity GaAs is $\lambda_{sc} = 46\ W/(mK)$, the specific heat capacity is $c_{sc} =$

350 $J/(kgK)$.[35] The mass of one solar cell can be determined based on the data sheet from that the: $m_{sc} = 0.00129\ kg$. From the mass and specific heat capacity, the heat capacity can be calculated by equation (20).

$$C_{sc} = m_{sc}c_{sc} = 0.454\frac{J}{K} \tag{20}$$

Except for the top and bottom panels, the dimension of one side panel is $46x46x1.6\ mm$,the corresponding material properties are shown table 5. Based on its dimensions, the mass of a PCB can be estimated as the volume multiplied by the density. The mass of one side is $m_{PCB} = 0.00643\ kg$. To derive the heat capacity, the mass is multiplied further with the specific heat capacity. Equation (21) shows the result.

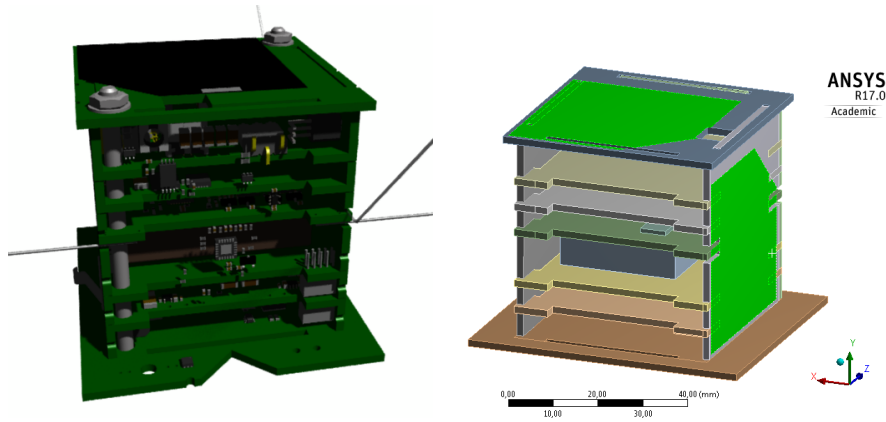$$C_{PCB} = m_{PCB}c_{PCB} = 6.432\frac{J}{K} \tag{21}$$

A RTV-S 691 type silicon based adhesive will be used to fasten the solar cells to the sides. The heat conductivity and specific heat capacity of silicon base adhesives are around $\lambda_{RTV} = 0.3\ W/(mK)$ and $c_{RTV} = 1250\ J/(kgK)$. The mass of the adhesive, calculating the volume under the solar cell with $0.5mm$ thick layer and multiplying it with $1410\ kg/m^3$ density yields: $m_{RTV} = 0.00106\ kg$. From this the heat capacity calculated by equation (22).

$$C_{RTV} = m_{RTV}c_{RTV} = 1.328\frac{J}{K} \tag{22}$$

By combining equation (20), (21) and (22) the total heat capacity of one side is:

$$C_{side} = C_{sc} + C_{PCB} + C_{RTV} = 8.214\frac{J}{K} \tag{23}$$

The solar cells provide the 5% of the heat capacity while the adhesive is repsonsible for 20% of that. At first, this may seem a lot but this is only one side, by determining it on the entire satellite, including the internal PCB sheets, battery and electrical components this would only be a very small portion of the heat capacity of the whole assembly. Neglecting the solar cells and the adhesive only moves toward safety because the larger heat capacity reducing the temperature fluctuation amplitude. In addition, the heat conduction through the three parts of a side panel in descending order: $\lambda_{sc} > \lambda_{RTV} > \lambda_{PCB}$ which implies that neither the solar cell nor the adhesive work as a heat insulator before the PCB. For this reason, these are not included in the FEM modell. However, since the emissivity of the solar cell and the PCB is different thus, do not absorb the same amount of heat from the external radiation, the surface of the sides were decomposed into two parts, shown in figure 17b. Later, we will set the boundary conditions up according to this consideration. Similarly, the threaded rods have also been ignored.

(a) The initial CAD geometry.　　　(b) The FEM model geometry

Figure 17: The geometric model.

7.1.2　Meshing

The meshing was done by the built-in mesher. The aim was that the sides are built with only one layer with hex-dominant quad elements because we did not want to examine the temperature distribution in the walls. But it is important that the side length of the elements is nearly the same and evenly distributed through the sides therefore the minimum side length of the elements is 1.6 mm, one from the six sides is shown in figure 18. This is necessary because of the temperature distribution in the plane of the plate directions perpendicular to the plate normal, directly affect the heat transfer between the sides. Of course, this also applies to the internal PCBs. The battery is also meshed with quad elements but with larger side lengths.
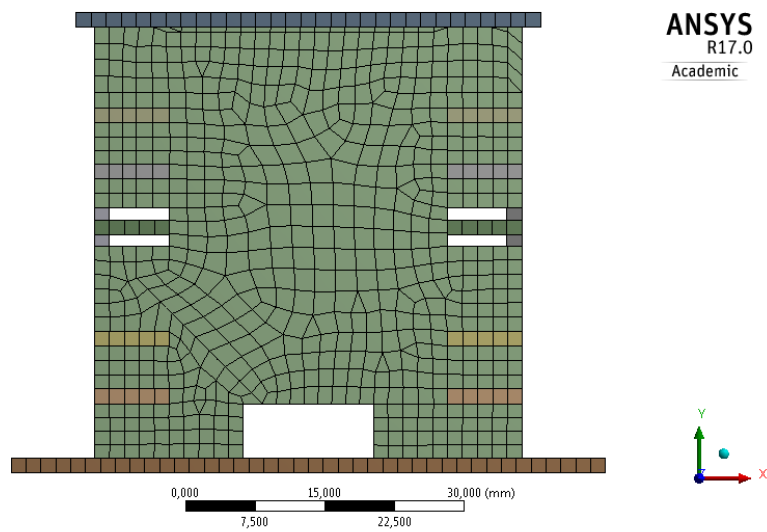

Figure 18: A meshed side.

7.1.3 Material data

The material data used for the analyses is summarized in table 5. These are general values mostly given for the Fr4 PCB while the battery material data is based on the lithium characteristics, except for the thermal conductivity which was deliberately set to a high conductivity value so that the battery itself has homogeneous temperature distribution. This way the heat resistance inside the battery is minimal, therefore, it responds quickly to the altering temperature.

Material	Density $\frac{kg}{m^3}$	Specific heat $\frac{J}{kgK}$	Thermal conductivity $\frac{W}{mK}$
FR-4 PCB	1900	1000	0.22
Battery	2770	1000	80

Table 5: Material data.

7.2 Boundary conditions

7.2.1 External heat load

As previously defined, a hot and cold case for the thermal environment in our orbit, now we define a geometrical hot and cold case. Although, as the satellites travels in its orbit the incidence of radiation coming from the Sun and the Earth constantly changing which is further affected by the six degress of freedom motion of the satellite. To determine this, it is practically impossible since it is not known how it will leave the deployer. For this reason, we used the simplification that in cold case the incidence of the radiation is normal to one of the satellite surface while in hot case the incidence of the radiation it is aligned with the cube diagonal. Therefore, in the cold case, the lowest surface area is considered, meaning the lowest absorbed heat. The hot case is when the heat flux is parallel to a diagonal of the cube. Thus, it is applied to an entire period, and the heat fluxes are calculated for this configuration by using equation (24) for the cold case and

equation (25) for the hot case.

$$S_{min,sc} = 0.73\ S_{min}\varepsilon_{sc}$$
$$S_{min,PCB} = S_{min}\varepsilon_{PCB}$$
$$LW_{PCB,d} = \varphi_d\varepsilon_{PCB}q_{LW,min}$$
$$LW_{sc,d} = \varphi_d\varepsilon_{sc}q_{LW,min}$$
$$SW_{PCB,d} = \varphi_d\varepsilon_{PCB}q_{SW,min}$$
$$SW_{sc,d} = \varphi_d\varepsilon_{sc}q_{SW,min}$$
$$LW_{PCB,s} = \varphi_s\varepsilon_{PCB}q_{LW,min}$$
$$LW_{sc,s} = \varphi_s\varepsilon_{sc}q_{LW,min}$$
$$SW_{PCB,s} = \varphi_s\varepsilon_{PCB}q_{SW,min}$$
$$SW_{sc,s} = \varphi_s\varepsilon_{sc}q_{SW,min}$$

$$\text{(24)}$$

$$S_{max,sc} = \cos(54.75)\varepsilon_{sc}0.73\ S_{max}$$
$$S_{max,PCB} = \cos(54.75)\varepsilon_{PCB}S_{max}$$
$$LW_{PCB,d1} = \varphi_{d1}\varepsilon_{PCB}q_{LW,max}$$
$$LW_{sc,d1} = \varphi_{d1}\varepsilon_{sc}q_{LW,max}$$
$$SW_{PCB,d1} = \varphi_{d1}\varepsilon_{PCB}q_{SW,max}$$
$$SW_{sc,d1} = \varphi_{d1}\varepsilon_{sc}q_{SW,max}$$
$$LW_{PCB,d2} = \varphi_{d2}\varepsilon_{PCB}q_{LW,max}$$
$$LW_{sc,d2} = \varphi_{d2}\varepsilon_{sc}q_{LW,max}$$
$$SW_{PCB,d2} = \varphi_{d2}\varepsilon_{PCB}q_{SW,max}$$
$$SW_{sc,d2} = \varphi_{d2}\varepsilon_{sc}q_{SW,max}$$

$$\text{(25)}$$

where:

- S is the heat flux in W/m^2 from the solar radiation, the max is for the hot case, the min is for the cold case. The sc and PCB in the lower index are the references for the solar cell and the PCB surfaces. The 0.73 multiplier comes from the solar cell efficiency which is 0.27 thus this portion of the solar radiation is transformed to electricity and the rest 0.73 becomes heat energy.

- LW and SW heat flux in W/m^2 is the longwave and shortwave radiation from the Earth radiation and the albedo flux. The first lower indexes are the surface type while the second is the view factor from figure 5, summarized in table 6.

- q is the calculated thermal environment by figures 15 and 16.

Of course, these variables are time-dependent, in fact, what we have done is that we multiplied the functions showed in figure 15 and 16. Therefore, equation (24) and (25) are not showed. Furthermore, the radiation from the Sun is a constant value on the

Normal to surface	notation	view factor
Angle between surface normal and zenith: 0°	φ_d	0.9
Angle between surface normal and zenith: 90°	φ_s	0.3
Angle between surface normal and zenith: 54.75°	φ_{d1}	0.73
Angle between surface normal and zenith: 144.75°	φ_{d2}	0.05

Table 6: View factor notation.

illuminated part of the orbit for 58 *min*. On the other 38 *min*, when the satellite is in Earth shadow, it is 0. The time change has been arranged together that at the cold case the start of the simulation is the time when the satellite is in the Earth shadow, while the hot case starts when the satellite is at the starting poing of the illuminated section. Figures 19 and 20 are shown to help the understanding the spatial position of the boundary conditions.
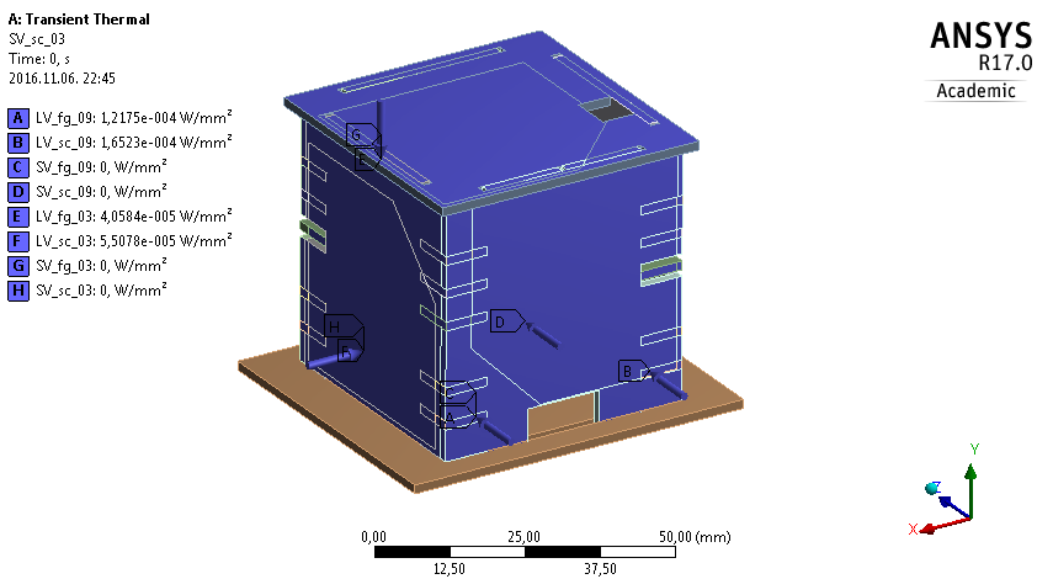
Figure 19: Boundary conditions in the cold case. A, B, C, and D are the LW and SW fluxes from the OLR and albedo radiation when the surface normal is aligned with the zenith direction. E, F, G, and H are the LW and SW fluxes from the OLR and albedo radiation when the surface normal is 90° from the zenith direction. The Sun radiation is not shown as it is in the opposite side of the cube.

7.2.2 Internal heat load

The internal heat generation is from the electronic components mainly from the COM chip and battery, enabled only in the hot case. The generated heat by the COM chip is the following:
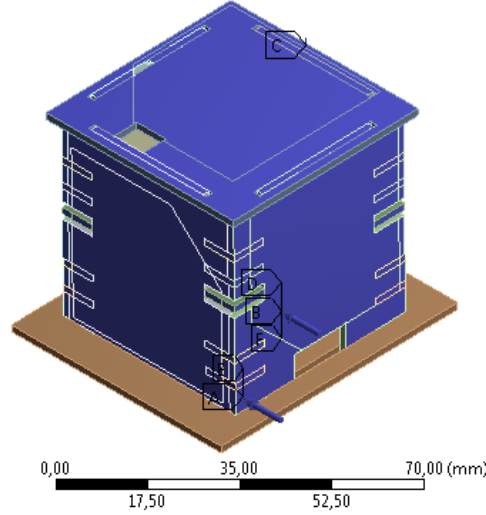
(a) A, B, C, D, E, and F is the Solar radiation, LW and SW fluxes from the OLR and albedo radiation when the direction of the is aligned with the cube diagonal.
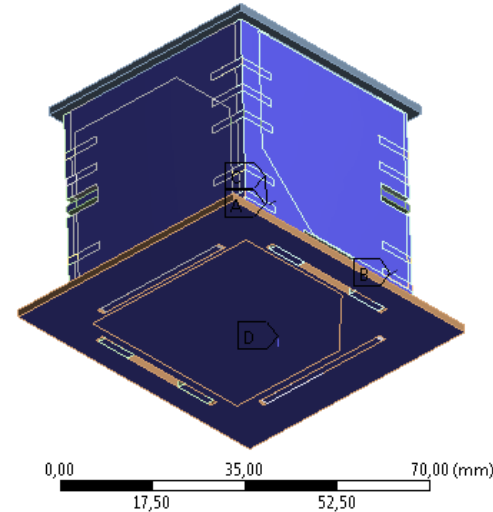

(b) A, B, C, and D in the LW and SW fluxes from the OLR and albedo radiation on the opposite side of the cube pointing to the Earth surface.

Figure 20: Boundary conditions in the hot case.

- at broadcasting: 240 mW

- at reception: 120 mW

The broadcast and reception ratio is 1:1 thus, the avarage power is 180 mW. The volumetric heat generation by the batter is 14 mW.

7.2.3 Internal heat distribution

Inside the satellite, the heat between the PCBs is transferred by radiation and conduction through the contact surfaces. The contact between the sides and the internal circuit boards are considered perfect as they are very tightly fit togeather. Figure: 21 shows the heat radiated between the internal components and the battery.
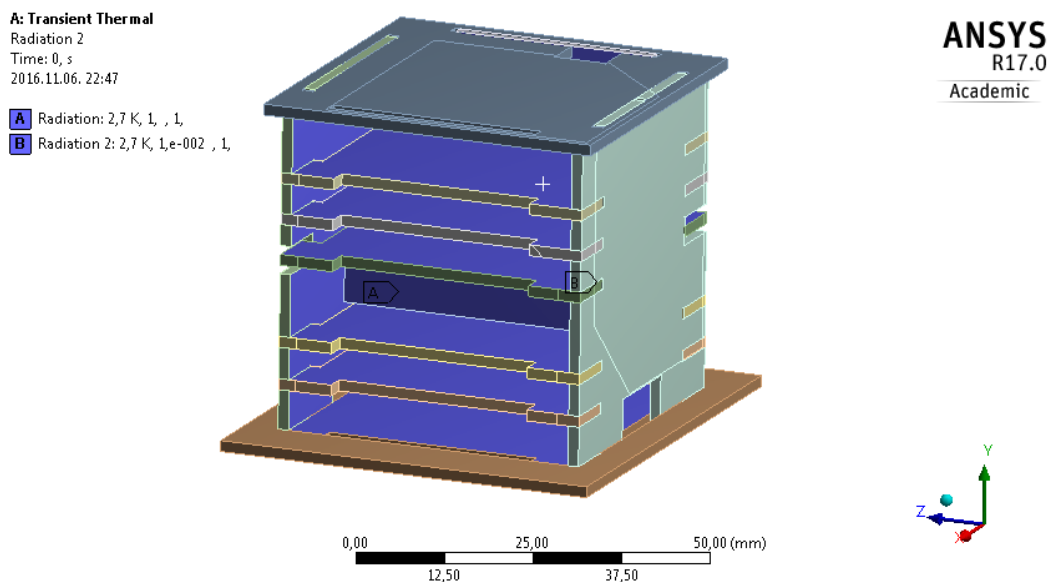

Figure 21: Radiation between the internal componenets.

7.2.4 The battery is directly mounted on the PCB

The original idea was that the battery, can be mounted on the COM subsystem board (the central panel in figure 3). Here, the chip is located in one side and the battery is on the other side of the PCB, shown in figure 22. Where the COM chip highlighted by blue and the battery by green color. Hence, the heat generated by the COM chip by broadcasting and receiving is transferred to the battery which is heated via the direct contact.
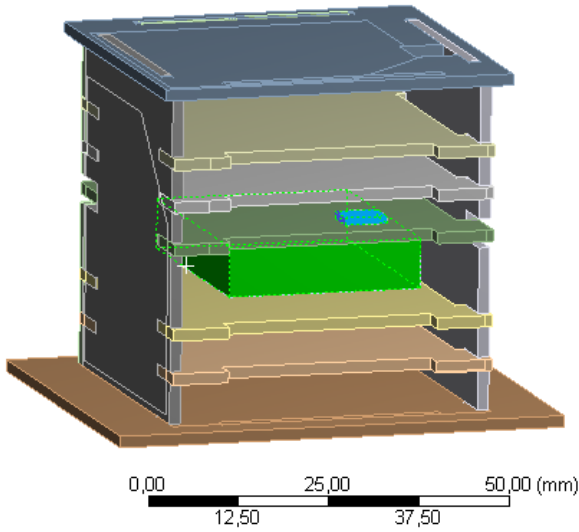
The main problem with this; that the battery must be in contact with the entire surface of the PCB. When the satellite is not broadcasting, the battery can quickly transfer its heat energy to the PCB which is transfers that further via condiction and radiation to the outer sides. Finally, the heat is transferred to the outer surfaces then to the space at 2.7 K temperature. This fact becomes crucial in the deployment phase. Since the first 20-30 minutes are scheduled radio silence to allow the satellites to gow the distance between each other and it happens in the shadow section, the battery temperature drops below 0 $°C$ in a fast way. The antenna opening system consists of two redundant resistors to melt the fishing line that holds the antenna closed. The procedure requires high electric power, therefore, it is mandatory to ensure battery temperature of 0 $°C$ or higher when the satellite is commanded to do so.

Figure 22: The arrengement of the battery and the COM chip.

Therefore, in this setup, a whole side of the battery is in a direct contact with the PCB. The simulations were run on three different emissivity insulation setups to investigate how this affects the battery temperature. The three emissivity values are: $\varepsilon = 1$ (the battery is not insulated), $\varepsilon = 0.01$ and $\varepsilon = 0.02$. The result of the cold cases is shown in figure 23. It can be seen that in this case, there is almost no difference between the various insulations. The temperature fluctuates between -50 $°C$ to -35 $°C$ it is inadequate for the operation of the battery. Figure 24 shows the hot case for this arrangement. Only the uninsulated simulation was investigated as hot case, because we were interested in the outcome but after the cold case, it is foreseeable that this arrangement is not appropriate for the satellite.
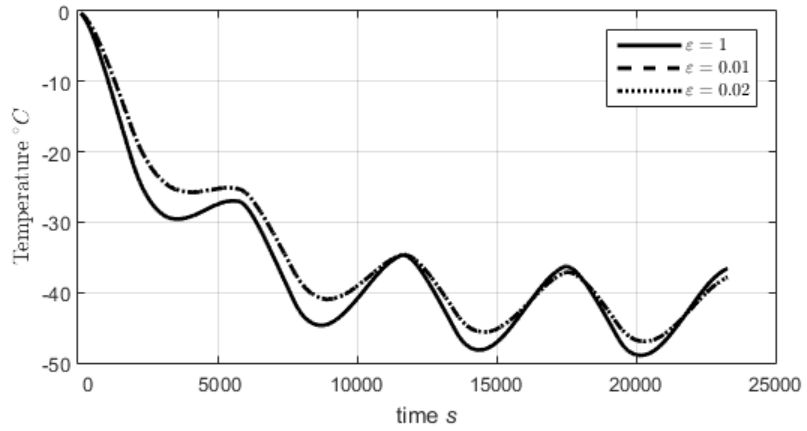
Figure 23: The battery temperature at the cold case when it mounted directly to the PCB.
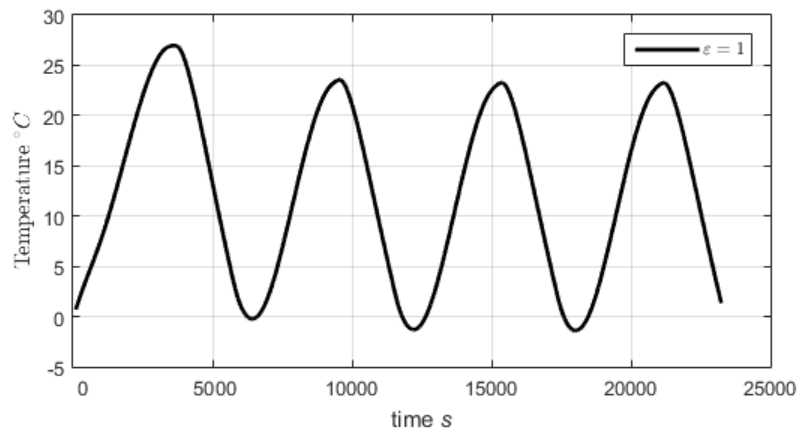

Figure 24: The battery temperature at the hot case when it mounted directly to the PCB.

7.2.5 Lifted battery by using spacers

To prevent the rapid cooling, the battery is lifted with; spacers in order to separate it from the other components and minimize the contacting surfaces between the battery and the PCB. As a consequence, a design-related problem arises to find the appropriate geometry and material. In general, all applied materials must comply with the Eropean Cooperation for Space Standardization (ECSS) standards, for material regulations: ECSS-Q-ST-70-02C. The organization is established in 1993 and its purpose is to provide standards in order to help the European space industry. Contractors working for ESA or European companies must adhere to this standards. However the selection of the right material is only be addressed in the next subchapter, here we examine how the spacer effects the battery temperature with different insulations.
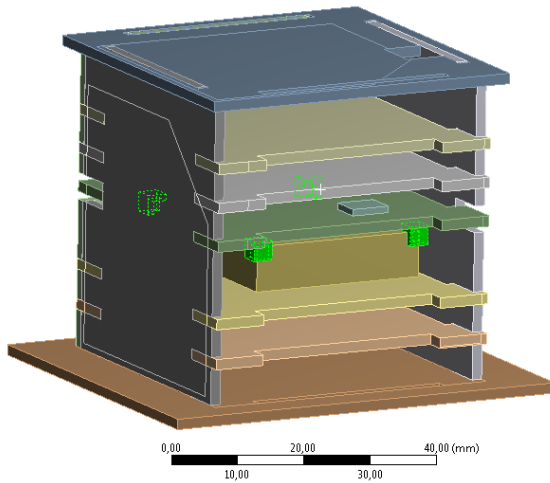

Figure 25: The arrengement of the spacers.

The determination of the spacer geometry and dimensions are determined by the available space with the need to minimize the contacting surfaces while ensuring that the battery is fixed inside the cap. The cap is made out of a 0.35 mm thick copper sheet and soldered to the PCB holding inside the battery. The available space between the two PCBs is 10.4 mm while the battery height is 7 mm. Thus we have approximately 3.4 mm to use. This is a bottleneck as that the battery is slightly bigger, because there is a Kapton tape around it to electrically insulate it from the PCB and do not forget the copper cap with thickness of 0.35mm. SConsequently, the available space is gross 3 mm. Based on this the spacer thickness should be 1mm and placed on the battery corners, lifting it up by 1mm from the PCB and the copper cap. The arrangement of the spacers is shown in figure 25 the spacer are highlighted by green. The contact surface is 9mm^2 with the PCB and 12mm^2 with the battery. As for the material data to be used, general plastic elements were considered as:

- $\lambda = 0.3 \ \frac{W}{mK}$ is the theramal conductivity,

- $c = 1600 \ \frac{J}{kgK}$ is thespecific heat,

- $\rho = 1500 \ \frac{kg}{m^3}$ is the density.

The results of the cold case is shown in figure 26, as for the hot case, in figure 27. It can be seen that the non-insulated (when the emissivity equals to one) and the insulated cases are now separated from each other. The temperature fluctuates between -42 °C to -38 °C which different from the previous one and still inadequate for the operation of the battery. At the hot case, the fluctuation is between 28 °C to 36 °C when it is insulated while without insulation, it is nearly the same shown in figure 27. So there is a reduction in the temperature amplitude, but the average temperature does not change much in the cold case. However, in the hot case with insulated battery, the temperature is high which is still within the temperature range of operability. Therefore, we recommend the spacers to use. Furthermore, the conclusion from the different emission cases above is that reducing it to lower than than 0.01, does not result in any significant changes. Based on this, the battery insulation can be improved by only increasing the contact thermal resistance.
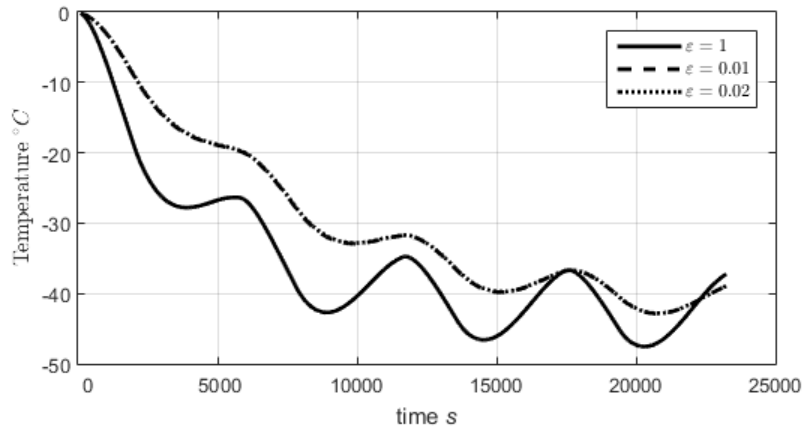

Figure 26: The battery temperature in the cold case when it placed on spacers.
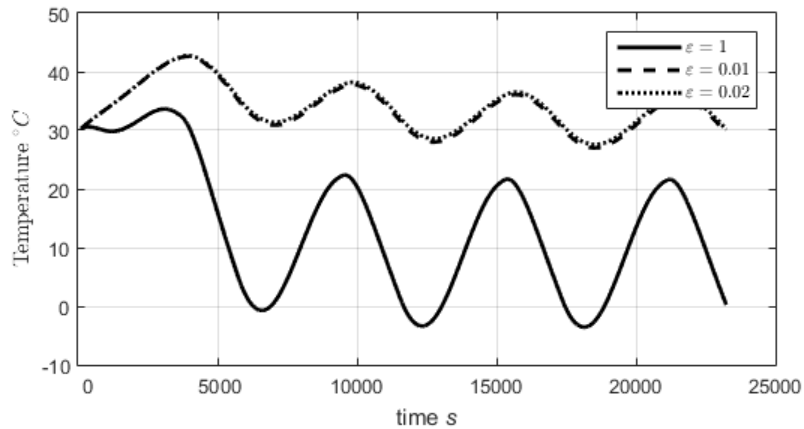

Figure 27: The battery temperature in the hot case when it placed on spacers.

7.2.6   Spacer material

The main aspects of the spacer material selection is to choose the lowest possible thermal conductivity material which meets the requirements of the ECSS. In general, the thermal conductivity of the plastics is low, and they are relatively easily to mill. The requirements related to polymer materials can be found in the Space product assurance of ECSS[25]. Two main criteria related to polymer materials is that the recovered mass loss (RML) and the collected volatile condensable material (CVCM) may not exceed the specified limitations. The CVCM by definition: „quantity of outgassed matter from a test specimen that condenses on a collector maintained at a specific temperature for a specific time" and the RML: „total mass loss of the specimen itself without the absorbed water". These are expressed as a percentage of the lost mass. So the point is that from materials like plastics, in the vacuum of space, the volatile gasses and absorbed water are subjected to released which might damage the electrical components and impair the effectiveness of the insulation. The permissible limits are:

- RML$< 1\%$

- CVCM$< 0.1\%$

After a brief survey, a company was found that deals with the manufacturing and machining os special plastics. As a result, the following materials met the above-detailed criteria:

- Ketron 1000 PEEK: $RML = 0.03\%$, $CVCM = 0.003\%$

- Ketron HPV PEEK: $RML = 0.02\%$, $CVCM = 0.003\%$

- Techtron 1000 PPS: $RML = 0.02\%$, $CVCM = 0.003\%$

Material	T_{max} $°C$	T_{min} $°C$	References
Ketron 1000 PEEK	250	-50	[36]
Ketron HPV PEEK	250	-20	[37]
Techtron 1000 PPS	220	-30	[38]

Table 7: Spacer material operation temperature ranges.

The operating temperature of the materials are shown in table 7. It is obvious that the maximum temperature limits are not exceeded. However, the minimum level is violated with the exception of the PEEK 1000. The material properties are shown in table 8. From simulation point of view, the notable differences between the materials is their

thermal conductivity. Although it is clear that the lowest thermal conductivity will be the best, but the simulation provides a comprehensive survey of how that affects the temperature of the battery. Thus, in a total of three different simulations that run, only the spacer material will vary while the emissivity of the battery is the same for all the cases at $\varepsilon = 0.02$. The results of the cold case is shown in figure 28, for the hot case, it is

Material	Density $\frac{kg}{m^3}$	Specific heat $\frac{J}{kgK}$	Thermal conductivity $\frac{W}{mK}$	References
Ketron 1000 PEEK	1310	$\cong 1300$	0.25	[36]
Ketron HPV PEEK	1450	$\cong 1300$	0.78	[37]
Techtron 1000 PPS	1350	$\cong 1300$	0.3	[38]

Table 8: Spacer material data

presented in figure 29. The results compared to the previous one do not show significant differences. Based on results and operating temperatures the best spacer material was PEEK 1000 out of the mentioned three candidates.
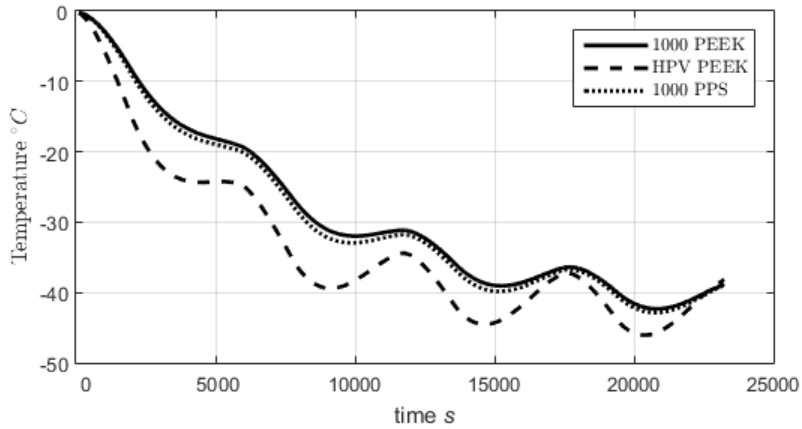

Figure 28: The battery temperature in the cold case by using various spacer materials.

7.2.7 Simulation summary

The isolation of the battery by spacers and thermal insulation actually reduce the amplitude of temperature fluctuations and the average value also increased by the thermal insulation. In the hot case, the battery remains in the operation range, but in the cold case, the batter temperature is out of the desired range. In the following, we take into account a different time averaging of the thermal environment which is closer to the real environment.
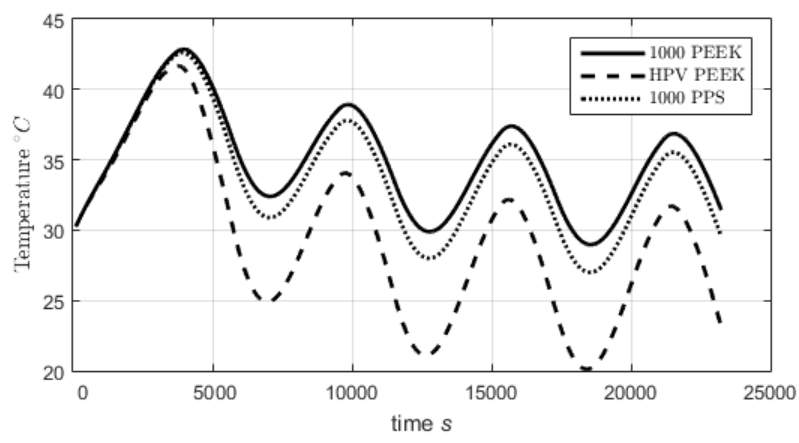
Figure 29: The battery temperature in the hot case by using various spacer materials.

8   Validation

The validation was performed in a thermal vacuum chamber. The chamber has been heated up to 65 $°C$ with the satellite in it. When the temperature was reached the desired value, a 60 W bulb was switched on and off in 5 minute intervals while an average 99 mW heat released from the COM chip by continuous broadcasting and receiving. According to this, we have carried out a simulation, and the results are shown in figure 30. Although it follows the measurement data reasonably well at the beginning which
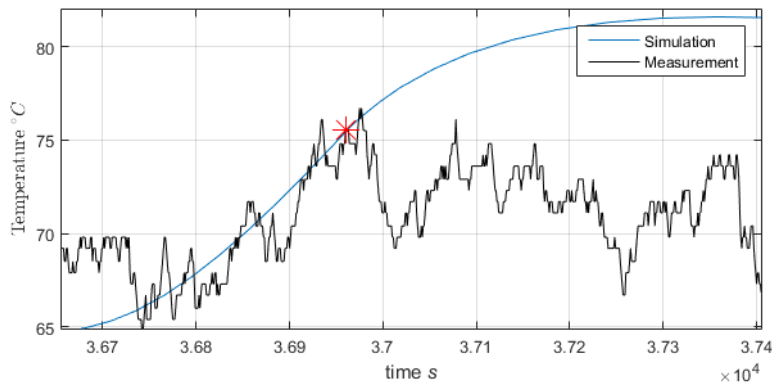

Figure 30: Validation of the satellite modell.

may seem good but through thinking about how much components have been neglected resulting in lesser heat capacity compared to the real satellite the calculated temperature should be above of the measurement. The red star shows the time when the light bulb was turned off. However, battery temperature in the simulation is still growing further which implies that the thermal conductivity of the PCBs is lower than in the simulated cases. Nevertheless, the contact resistances also affect the results.

9 FEM analisys of the detailed model

In order to get closer to the reality with our model, the geometry ,boundary conditions and material properties have to be modified. For the geometry, the electronic equipments are taken into account because of their heat capacity and the heat tranfer between the sides and the internal components. Unfortunately, as it was not possible to measure the thermal conductivity and heat capacity of either the PCB with the mounted circuit components and the battery, the values were taken from the literature, resulting in a more accurate setup than those used previously. The boundary conditions are calculated with longer averaging time which yields a more realistic approximation of the thermal environment in the SMOG-1 orbit.

9.1 Geometry

The copper cap holding the battery and all the spacers were added to detailed model.

9.1.1 Estimated properties of the electronic components

Figure 31 shows the mass measurement of the satellite without the battery. Besides that, the PCB side panels were also measured separately. From the latter, the PCB density was calculated resulting in roughly $\rho_{PCB} = 2400 \ kg/m^3$. This can be used to determine the total mass of the side, top, bottom and internal PCBs shown in table 31. Subtracting
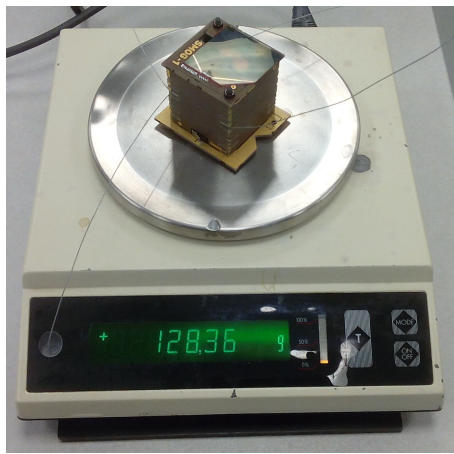
Figure 31: The measurement of the satellite without the battery and with only one solar cell mounted.

the calculated mass and the solar cell mass from the measured value yields the total mass of the electronical components, as shown in, equation (26).
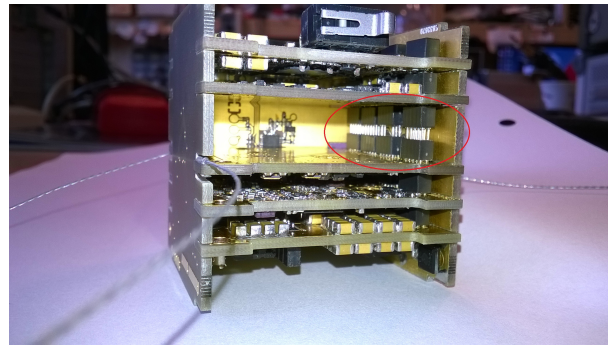
$$m = 128.36 - 2.59 - 86.28 = 39.49 \ g \tag{26}$$

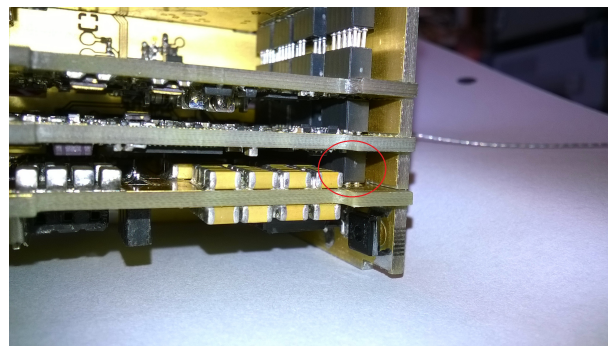| Panel	Quantity	Volume mm^3	Mass g	Total mass g
Sides	4	3131	7.514	37.5
Internal	5	2808	6.74	33.7
Top	1	3599	12.9	12.9
Bottom	1	5410	8.63	8.63

Table 9: Mass of the PCBs.

So the electrical components are modeled as sheets and placed on the internal components such a way that their heat capacity is equal to the silicon dioxide specific heat multiplied by the calculated mass of the electronics. In other words: the heat capacity of the plates is equal to the estimated heat capacity of the internal electrical components.

9.1.2 Heat transfer between the internal components

All the internal panels connected to each other by the power bus, while the side panels are connected to the internal system by three wire. The question that arises is how this affects the internal components. The sides are in contact with the internal components in a relatively large surface compared to the three small wires. Therefore, the wires do not significantly affect the heat flow thus it can be neglected from the simulation. However, the internal panels are not in a direct contact with each other, the only link between them is the bus connector. Figure 32 shows the SMOG-1 internal components and the bus connector. In order to determine that it significantly affects the heat transfer or not, we created two separate simulations, shown in figure 33. Figure 33a shows the case with the bus connectors which allows thermal conduction. Beside that there is a radiation boundary condition. The second simulation is shown in 33b which consists of only a radiative thermal contact. The input boundary conditions are the same but their value is not important. What matters is that one of the two sheets has a heat flux while the other radiate to the ambient. Since the boundary conditions are the same in both cases, comparing the temperature of the two simulations show the effect of the bus connector. Figure 34 shows the free side temperature, and it can be seen that the difference is significant. For this reason, we add thess pins to the detailed simulation.

(a) The power bus conecting the internal PCBs.

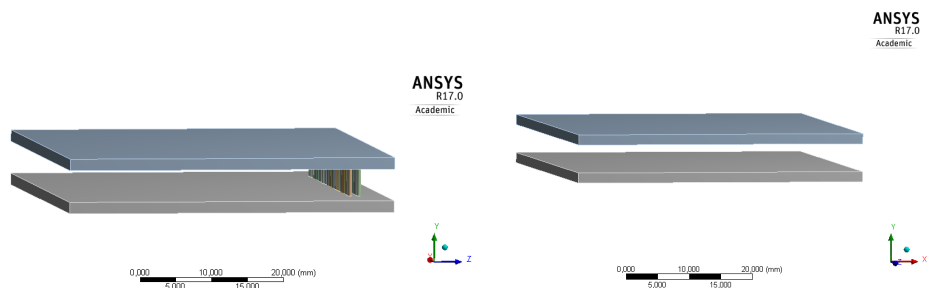(b) The power bus conecting the internal PCBs.

(c) g to the surface.

Figure 32: The electrical connecting between the internal PCBs and the side panels.

(a) Test geometry with the bus connector pins.

(b) Test geometry without the bus connector pins.

Figure 33: Test geometry of the power bus heat conduction between the internal panels.
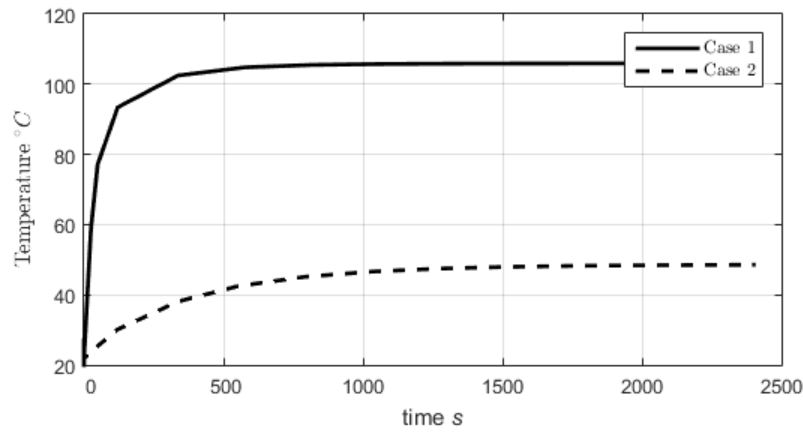
Figure 34: The temperature of the sheets, where case 1 is the sheets with the bus connector, case 2 is the sheets without the bus connector.

9.1.3 Battery positioning

Figure 35 shows the geometry of the spacers and the battery inside the copper cap. Compared to the previous simulation, we have changed the geomerty of the spacers.
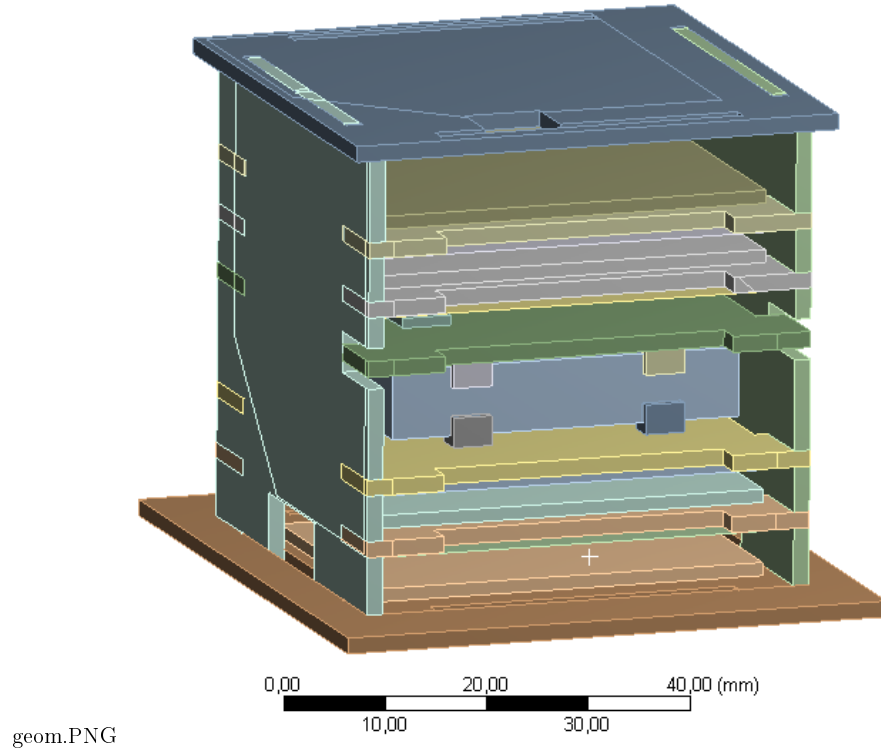

geom.PNG

Figure 35: Deatailed geometry model of the satellite.

42

9.2 Material data

The material data is summarized in table 10. This time the thermal conductivity of the PCB is anisotropic because in the direction of the plate normal its conductivity is lower than in the other two directions because of the composite material structure. The thermal properties of the battery are taken from a paper while the density is measured in the same was as the PCB was. The properties of the copper are used for the pin and the cap while the silicon dioxide is for the electrical components.

Material	Density $\frac{kg}{m^3}$	Specific heat $\frac{J}{kgK}$	Thermal conductivity $\frac{W}{mK}$	References
Copper	8790	386	401	[27] [28] [29]
FR-4 PCB	2400	1200	normal to plane: 0.35 ,in plane: 0.81	[31] [30]
Silicon dioxide	2170	680	1.3	[26]
Lithium ion battery	2057	1250	3	[32]

Table 10: Material data.

9.3 Boundary conditions

Now we want to examine the difference in temperature resulting from the satellite angular velocity around of its own axis. This is done by instead of using a cold and hot case heat flux we use only one for two simulations where the difference is only the affected surface area. The chosen values are from table 2, it is the combined extreme type with 24 hour averaging time. This value is much closer to the expected conditions. So the same heat flux affects the minimum case where the radiation incidence is normal to the surface, the maximum case is when the radiation incidence is aligned with the cube diagonal. The internal heat load is the same it was in the previous simulations.

9.4 Results and summary

Figure 36 shows the results of the simulation. Although, after simulating three orbital periods, the temperature is still not show a quasi-steady behavior but it tends to that. Thus, it is expected that in the case of a general 3D motion, the battery temperature is somewhere between the two functions. Despite our efforts, the temperature of the battery still can fall below sub zero temperatures. However, the heat flow between the battery and the spacers are still assumed to be perfect. Nevertheless, the thermal resistance is higher since the battery is surrounded with a heat insulation film. This setup will be calculated in a later time and exceeds the limitation of the present paper.
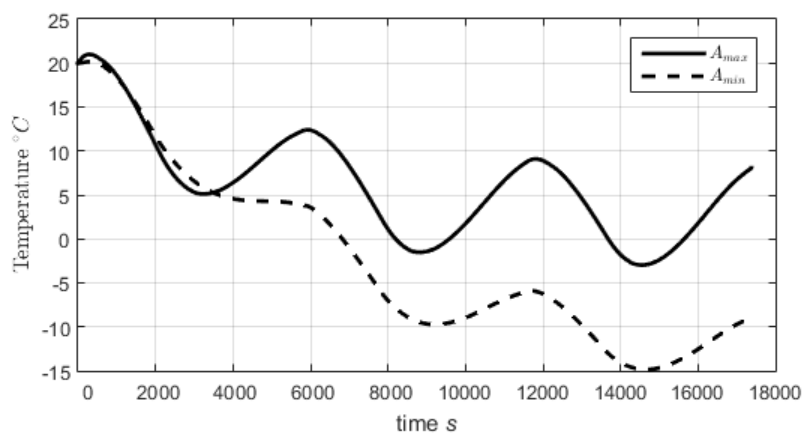
Figure 36: The detailed model battery temperature.

10 Progress and future directions

It can be seen that we made significant progress during the last one year. However, only a portion is included in the present paper due to the lack of time. Since the orbit of the SMOG-1 has been determined, the thermal environment could be determined. The spacers ordered and the heat insulation has arrived from Dunmore corporation. So, slowly, we can assembly the battery according to the results.

However, we have to face it that based on the calculation, the battery temperature can exceed the minimum value. In addition, there are problems with the validation of the FEM model because our university does not have appropriate vacuum chamber to test the satellite insulation. This applies even to the insulation films as their heat resistance can only be measured in thermal vacuum conductivity meter, but we do not have this kind of instrument.

Of course, it is a viable option to freeze the satellite then put into a simple vacuum chamber at room temperature and measure the time until it heats up. Now, based on the results of the present work, I neglect the further simulations and put more emphasis on the validation and thermal testing of the satellite.

11   References

[1] Dudás Levente, *The Spectrum Monitoring System of Smog-1 Satellite*, MAREW 2015

[2] Timur Kristóf , *A SMOG-1 PocketQube muhold redundáns fedélzeti számítógépének hardver és szoftver fejlesztése*, BME TDK 2015

[3] Herman Tibor, *A Smog-1 PocketQube elsődleges energiaellátó rendszere*, Msc thesis 2015

[4] Géczy Gábor, *Smog-1 műhold központi energiaellátó rendszer és kísérleti doziméter tervezése*, TDK 2015

[5] Géczy Gábor, *A SMOG-1 PocketQube másodlagos energiaellátó rendszere*, Msc thesis 2016

[6] The official home of the PocketQub standard, *pocketqub standard*, https://pocketqub.wordpress.com/standard/, last accessed: 2015.09.20 17:33

[7] Maria M. Garzon, *Development and analisys of the thermal design for the Osiris-3U CubeSat*, Thesis 2012

[8] Joe Bauer, Michael Carter, Kaitlyn Kelley, Ernie Mello, Sam Neu, Alex Orphanos, Tim Shaffer, Andrew Withrow, *Mechanical, Power, and Thermal Subsystem Design for a CubeSat Mission*, Bsc Thesis 2012

[9] Dai Q. Dinh, *Thermal modeling of nanosat*, Bsc Thesis 2012

[10] Sylwia Czernik, *Design of the Thermal Control System for Compass-1*, Diploma Thesis 2004

[11] S. Corpino, M. Caldera, F. Nichele, M. Masoero, N.Viola, *Thermal design and analisys of a nanosatellite in low earth orbit*, Acta Astronautica 115 (2015) 247-261

[12] Murat Bulut, Nedim Sozbir, *Analytical investigation of a nanosatellite panel surface temperatures for different altitudes and panel combinations*, Applied Thermal Engineering 75 (2015) 1076-1083

[13] Jáger Dávid, Török Péter, *PocketQube műhold numerikus hőtani szimulációja*, BME TDK 2014

[14] Lionel Jacques, *Thermal Design of the Oufti-1 nanosatellite*, MSC Thesis 2009

[15] Gróf Gyula, *Hőközlés*, Budapest, 1999

[16] B.J. Anderson, C.G. Justus, G.W. Batts, *Guidelines for the Selection of Near-Earth Thermal Environment Parameters for Spacecraft Design*, NASA, 2001

[17] B.J. Anderson,B.F. James, C.G. Justus, G.W. Batts, *Simple Thermal Environment Model (STEM)*, NASA, 2001

[18] D. Gilmore, *Spacecraft Thermal Control Handbook: Volume I: Fundamental Technologies* , 2nd ed. 2002.

[19] Wertz, J. R., & Larson, W. J., *Space Mission Analysis and Design* , 3rd ed. 2005.

[20] G. Smoot, G. De Amici, S. D. Friedman, C. Witebski, N. Mandolsei, R. B. Partridge, G. Sironi, L. Danese, G. De Zotti, *New multifrequency measurement of the spectrum of the cosmic background radiation* , Adv. Space Res. Vol.3, No.10-12, pp.465-467, 1984

[21] S.K. Solanki, M. Fligge, *Solar irradiance variations and climate* , Journal of Atmospheric and Solar-Terrestrial Physics 64, 677-685, 2002

[22] T.H. Vonder Haar, G.G. Campbell, E.A. Smith, A. Arking, K. Coulson, J. Hickey, F. House, A. Ingersoll, H. Jacobowitz, L. Smith, L. Stowe, *Measurements of the earth radiation budget from satellites during the first garp global experiment* , Adv. Space Res. Vol.1, pp.285-297, 1981

[23] Eric A. Smith, *Orbital Mechanics and Analytic Modeling of Meteorological Satellite Orbits* Department of Atmospheric Science Colorado State University, 1980

[24] Mark Z. Jacobson, *Fundments of atmospheric modeling* Cambridge University press, 2005

[25] ECSS, *Thermal vacuum outgassing test for the screening of space materials* ECSS-Q-ST-70-02C, 2008

[26] AZoM.com, *Silica - Silicon Dioxide (SiO2)*, http://www.azom.com/ properties.aspx?ArticleID=1114, last accessed: 2016.08.27 18:44

[27] The engineering toolbox, *Density, Specific Weight and Specific Gravity* , http://www.engineeringtoolbox.com/density-specific-weight-gravity-d_290.html, last accessed: 2016.08.28 20:13

[28] The engineering toolbox, *Specific Heat of common Substances* , http://www.engineeringtoolbox.com/specific-heat-capacity-d_391.html, last accessed: 2016.08.28 20:13

[29] The engineering toolbox, *Thermal Conductivity of some common Materials and Gases* , http://www.engineeringtoolbox.com/thermal-conductivity-d_429.html, last accessed: 2016.08.28 20:13

[30] K. Azar, J. E. Graebner (1996). *Experimental Determination of Thermal Conductivity of Printed Wiring Boards* Proceedings of the Twelfth IEEE SEMI-THERM Symposium: 169–182.

[31] Dielectric corporation, *G 10 FR4 G 11(Glass Epoxy)General Material Properties*, http://www.dielectriccorp.com/downloads/thermosets/glass-epoxy.pdf, last accessed: 2016.08.28 21:25

[32] Iopscience, *Simplified Heat Generation Model for Lithium ion battery used in Electric Vehicle*, http://iopscience.iop.org/article/10.1088/1757-899X/53/1/012014/pdf, last accessed: 2016.08.27 9:25

[33] ThermoWorks, *Emissivity Table*, http://www.thermoworks.com/learning, last accessed: 2016.08.27 9:45

[34] Quioptic, *Solar Cell Coverglasses Designed and manufactured to provide radiation protection* http://www.azurspace.com/index.php/en/, last accessed: 2016.08.27 9:54

[35] ISP optics, *Gallium Arsenide (GaAs)* www.ispoptics.com, last accessed: 2016.10.25 10:54

[36] QUADRANT Engineering Plastic Products, *Ketron 1000 PEEK*,

[37] QUADRANT Engineering Plastic Products, *Ketron HPV PEEK*,

[38] QUADRANT Engineering Plastic Products, *Techtron 1000 PPS*,